



1 **European sulphate aerosols were a key driver of the early**  
2 **twentieth-century intensification of the Asian summer monsoon**

3  
4 Weihao Sun<sup>1,2</sup>, Massimo A. Bollasina<sup>1</sup>, Ioana Colfescu<sup>3,4</sup>, Guoxiong Wu<sup>2</sup> and Yimin Liu<sup>2</sup>  
5

6 <sup>1</sup>School of GeoSciences, University of Edinburgh, Edinburgh, UK

7 <sup>2</sup>Key Laboratory of Earth System Numerical Modelling and Application, Institute of Atmospheric Physics,  
8 Chinese Academy of Sciences, Beijing, China.

9 <sup>3</sup>School of Mathematics and Statistics, University of St Andrews, St Andrews, UK

10 <sup>4</sup>National Centre for Atmospheric Science, UK  
11

12  
13 Correspondence to: Massimo A. Bollasina ([Massimo.Bollasina@ed.ac.uk](mailto:Massimo.Bollasina@ed.ac.uk))  
14  
15

16 **Abstract.** Observations show that the Asian summer monsoon experienced substantial multi-decadal changes  
17 during the early 20<sup>th</sup> century, including a wetting trend over South Asia and a southward rainfall shift over East  
18 Asia. Despite their significance, these variations have received limited attention, and the underlying mechanisms  
19 remain poorly understood. This study investigates the role of increased European sulphate aerosol emissions in  
20 shaping these monsoon changes using ensemble experiments with the Community Earth System Model. The  
21 aerosol-driven rainfall patterns over South and East Asia resemble observations, suggesting that European  
22 aerosols played an important role in modulating the monsoon. These changes are linked to large-scale anomalies  
23 in surface climate and three-dimensional atmospheric circulation across the Indo-Pacific, which alter moisture  
24 transport to the continent, the main driver of the rainfall anomalies. Regional circulation anomalies form part of a  
25 hemispheric upper-tropospheric wave train originating over central Europe and extending through the Middle East  
26 to the Pacific. The wave train arises as a thermodynamic adjustment to the aerosol-induced surface cooling and  
27 related anticyclone over Europe, extends to the upper troposphere, and, while propagating eastward, induces three-  
28 dimensional circulation anomalies across Asia that affect the monsoon. These findings provide compelling  
29 evidence for the influence of European sulphate aerosols on the early 20<sup>th</sup>-century monsoon variability, which is  
30 relevant for improving current understanding of the regional-scale impacts of anthropogenic aerosols. As  
31 European SO<sub>2</sub> emissions continue to decline, this study sheds light upon a possible ongoing and future pathway  
32 which may significantly modulate the monsoon response to Asian aerosol changes.



## 33    **1 Introduction**

34    The Asian summer monsoon (ASM) is a vital source of water for over 60% of the world's population (Turner and  
35    Annamalai, 2012). Its interannual variability and long-term changes have significant implications for water  
36    resources, agriculture, and economic activities across Asia (e.g., Gadgil and Rupa Kumar, 2006).

37

38    In the past decade, anthropogenic aerosols have attracted considerable scientific interest due to their ability to  
39    offset part of the warming caused by greenhouse gases (GHGs) (e.g., Samset et al., 2018; Hegerl et al., 2019; Li  
40    et al., 2022). Aerosols influence climate by scattering and absorbing solar radiation, and by acting as cloud  
41    condensation and ice nuclei, thereby modifying cloud albedo, lifetime, and precipitation processes (Boucher et  
42    al., 2013; Stier et al., 2024). They remain the largest source of uncertainty in estimating anthropogenic climate  
43    forcing since the pre-industrial era (Andrews and Forster, 2020; Bellouin et al., 2020). While their global historical  
44    effective radiative forcing is smaller than that of GHGs, aerosols can trigger strong regional climate responses due  
45    to their spatial and temporal variability (e.g., Szopa et al., 2021).

46

47    The link between long-term changes in aerosol emissions and ASM variability is widely debated (e.g., Lau 2016;  
48    Li et al., 2016; Wu et al., 2016). Research is particularly challenging due to the compounding effects of internal  
49    variability, model biases, and divergent model responses (e.g., Saha and Gosh, 2019; Liu et al., 2024).  
50    Nonetheless, studies using observational and modelling evidence have highlighted the significant impact of  
51    aerosols, both regional (i.e., Asian-only) and remote (i.e., outside Asia), on the late 20<sup>th</sup> century weakening of the  
52    South ASM and the emergence of a southern-flood-northern-drought (SFND) pattern over East Asia (e.g.,  
53    Bollasina et al., 2011; Guo et al., 2013; Salzmann et al., 2014; Li et al., 2015; Dong et al. 2019; Wilcox et al.  
54    2020).

55

56    Gauge records reveal clear multi-decadal variability in both South Asian and East Asian summer monsoons  
57    throughout the 20<sup>th</sup> century (e.g., Zhang and Zhou, 2011; Preethi et al., 2017; Li et al., 2023). In particular, the  
58    first half of the century saw an increase in rainfall over South Asia, most notably in central India, and a tripole  
59    pattern over East Asia, with excess rainfall in the south and northeast, and drier conditions along the Yangtze River  
60    basin. These anomalies appear to be part of a coherent ASM-wide fluctuation, mirrored in broader NH summer  
61    monsoon changes (Zhang and Zhou, 2011; Preethi et al., 2017; Wang et al., 2018; Goswami et al., 2023).



62 Strikingly, this pattern reversed in the second half of the 20<sup>th</sup> century, producing comparable but opposite sign  
63 anomalies, and resulting in minimal net change over the full period.

64

65 While monsoon changes since the 1950s have been extensively studied (e.g., Bollasina et al., 2011; Salzmann et  
66 al., 2014; Song et al., 2014; Liu et al., 2019; Liu et al., 2024; Shao et al., 2024), early-century variations have  
67 received less attention. Yet, given the contrasting trends throughout the historical period, understanding monsoon  
68 drivers and the underpinning physical mechanisms in the entire record is essential to constrain the nature of its  
69 multi-decadal variability and improve future projections. This is particularly relevant in the context of  
70 disentangling internal climate variability from externally-forced changes (e.g., Salzmann and Cherian, 2015;  
71 Huang et al., 2020). In this regard, compared to the later period, it is conceivable to assume a negligible role of  
72 Asian aerosols in the first half of the 20<sup>th</sup> century, as emissions underwent a significant growth only from the  
73 1950s and a sharp rise after the 1970s (Smith et al., 2011; Lund et al., 2019). In contrast, North American and  
74 European aerosols had already increased substantially, raising the possibility of their significant influence on the  
75 monsoon.

76

77 Several studies have highlighted the potential role of remote, including European, aerosols in driving monsoon  
78 changes (e.g., Cowan and Cai, 2011; Bollasina et al., 2014; Guo et al., 2015; Dong et al., 2016; Liu et al., 2018;  
79 Shawki et al., 2018; Undorf et al., 2018a,b; Westervelt et al., 2018; Wang et al., 2020). However, these analyses  
80 often relied on idealised simulations, such as long equilibrium experiments with present-day emissions turned on  
81 or off. Whether aerosol influences were already detectable in the early 20<sup>th</sup> century remains an open question.  
82 Addressing this gap is crucial for better understanding and narrowing uncertainty in aerosol-related future  
83 monsoon projections, especially considering divergent present-day emission trends (e.g., Wang et al., 2021a) and  
84 a wide range of plausible future pathways (Samset et al., 2019; Persad et al., 2023).

85

86 Against this backdrop, this study investigates whether rising European sulphate aerosols – the dominant  
87 anthropogenic aerosol species of the region (e.g., Hoesly et al., 2018) – had any detectable impact on the ASM  
88 during the first half of the 20<sup>th</sup> century. Section 2 introduces the climate model, experimental setup, and  
89 observational data used. Section 3 presents the ASM response and examines the underlying mechanism.  
90 Discussion and conclusions are provided in Section 4.



91

## 92 **2 Data and methods**

93 The primary data comprises output from two transient historical (1850–2005) experiments with the fully coupled  
 94 Community Earth System Model (CESM) version 1.2.2 (Hurrell et al., 2013). The atmospheric component is the  
 95 Community Atmospheric Model version 5.3 (CAM5.3, Neale et al., 2012), which includes a 3-mode aerosol  
 96 scheme and a prognostic representation of aerosol-cloud interactions (Ghan et al., 2012). The horizontal  
 97 resolutions are  $1.9^\circ \times 2.5^\circ$  for the atmosphere and  $0.6^\circ \times 0.9^\circ$  for the ocean. The model reproduces spatial patterns  
 98 and magnitude of the climatological summertime monsoon rainfall and low-tropospheric circulation reasonably  
 99 well (Supplementary Fig. S1), consistent with the overall performance of CMIP5/CMIP6 models (Meehl et al.,  
 100 2020; He et al., 2023). A full description of the model and experiments is provided by Undorf et al. (2018a); here,  
 101 we briefly summarise key details.

102

103 Each experiment consists of an 8-member ensemble initialised from different points in a 200-year pre-industrial  
 104 (PI) simulation with fixed anthropogenic emissions at 1850 levels. The first experiment (ALL) includes time-  
 105 varying historical emissions of anthropogenic aerosols, greenhouse gases, and natural forcing factors. The second  
 106 (fixEU) is identical to ALL except that anthropogenic  $\text{SO}_2$  and  $\text{SO}_4$  emissions over Europe (EU) are held at PI  
 107 levels. Europe is defined according to Tier 1 regions from the Hemispheric Transport of Air Pollution 2  
 108 experiments (Koffi et al., 2016).

109

110 Several observational datasets are also used. Precipitation was taken from three land-only monthly gridded gauge-  
 111 based datasets to account for uncertainties and discrepancies: the  $1^\circ \times 1^\circ$  Global Precipitation Climatology Centre  
 112 v2020 (GPCC; Schneider et al., 2014), the  $0.5^\circ \times 0.5^\circ$  Climate Research Unit v4.00 (CRU; Harris et al., 2014),  
 113 and the  $0.5^\circ \times 0.5^\circ$  University of Delaware v401 (UDEL, Willmott and Matsuura, 1995). Monthly sea level  
 114 pressure surface is from the  $5^\circ \times 5^\circ$  Hadley Centre Sea Level Pressure dataset (HadSLP2; Allan and Ansell, 2006),  
 115 and 850-hPa winds from the ECMWF Reanalysis 5 (Hersbach et al., 2020). Monthly observed precipitation from  
 116 the  $2.5^\circ \times 2.5^\circ$  Climate Prediction Center Merged Analysis of Precipitation dataset (CMAP, Xie and Arkin, 2017)  
 117 is also used for model validation.

118



119 The analysis focuses on the summer (June–August, JJA) monsoon variation during the early 20<sup>th</sup> century.  
 120 Temporal changes are estimated using least-squares linear trends from 1901 to 1955. Alternative trend estimation  
 121 methods (i.e., Sen’s non-parametric slope or differences between the 1941–1955 and 1901–1915 means) yield  
 122 similar results (not shown). As the main objective is to isolate the influence of external forcing, particularly  
 123 anthropogenic aerosols, on the ASM, changes are primarily assessed using ensemble means. Assuming linear  
 124 additivity of responses, the difference between the ALL and fixEU experiments is interpreted as the impact of  
 125 European SO<sub>2</sub> emissions. Statistical significance is assessed using a two-tailed Student’s *t*-test at the 90%  
 126 confidence level. To identify the contribution of the model’s internal variability to the forced response, individual  
 127 ensemble members are also examined. Additionally, the PI simulation is used to assess the statistical significance  
 128 of the forced changes relative to internal variability. We generate 10,000 bootstrap samples of 8-member ensemble  
 129 means to construct the probability distribution of unforced linear trends; the 90% confidence interval is defined  
 130 as the range within which 90% of these fall.

### 131 **3 Results**

#### 132 **3.1 Observed and simulated precipitation trends**

133 Observational data show that JJA precipitation changes across Asia during the first half of the twentieth century  
 134 exhibit a coherent large-scale pattern (Fig. 1a), with robust features across multiple datasets (Supplementary Fig.  
 135 S2). Over South Asia, significant wetting is observed across central and northern India, contrasted by drying over  
 136 southern and northeastern India, the eastern Himalayas and northern Myanmar. Further east, rainfall deficits occur  
 137 over southern Indochina and Indonesia, with a pronounced drying over the middle and lower reaches of the  
 138 Yangtze River valley (105°–120°E, 25°–35°N). In contrast, precipitation increases are seen in a band extending  
 139 from northern Indochina through southern China, and further north into northwestern China and the Korean  
 140 peninsula. Interestingly, the anomalous rainfall pattern over South Asia closely resembles, but with opposite sign,  
 141 that associated with the late 20<sup>th</sup> century weakening of the monsoon, while the anomalies over eastern Asia are  
 142 reminiscent of the reversed SFND pattern (e.g., Bollasina et al., 2011; Dong et al., 2016).

143

144 To provide further context on the long-term precipitation variations, Figure 1c shows the observed time series of  
 145 monsoon rainfall anomalies over the core Indian monsoon region (75°–87°E, 16°–27°N land-only points, see box  
 146 in Fig. 1c). Beyond interannual and decadal fluctuations, the record reveals a marked increase from the 1900s to



147 the mid–1950s ( $+0.55/+0.76$  mm day<sup>-1</sup> in GPCC/CRU over 55 years, statistically significant at the 90% confidence  
 148 level), equivalent to about 7–11% of the long-term climatology. The anomaly also results in a 5–7% increase in  
 149 the All–India rainfall relative to early–century values. A similar analysis over southern China (110°–120°E, 25°–  
 150 35°N; Supplementary Fig. S3) also shows a prominent, statistically significant, multi-decadal trend.

151

152 Despite its coarser resolution, the ALL ensemble mean captures the main spatio-temporal characteristics of the  
 153 observed precipitation trends (Fig. 1b). The model reproduces the widespread precipitation increase over northern  
 154 India, albeit with a weaker magnitude ( $+0.14$  mm day<sup>-1</sup> (55 years)<sup>-1</sup> over the core region) and a slight eastward  
 155 shift, and the drying over southern India. The model likely underrepresents the full extent of the interaction with  
 156 the Western Ghats. The simulated rainfall dipole over eastern China aligns with observations, although the  
 157 amounts are slightly underestimated. However, the model fails to reproduce the wetting over southern China and  
 158 northern Indochina, possibly due to limitations in resolving interactions with the complex terrain. The sign of the  
 159 core precipitation anomalies over India is consistent across most of the individual ensemble members (6 out of  
 160 8), supporting a dominant anthropogenic origin (Supplementary Fig. S4).

161

162 Preventing European sulphate aerosols from increasing results in drier conditions over central-northern India and  
 163 the northern BoB, with wetting over the eastern Himalayas and Myanmar. Concurrently, the precipitation  
 164 anomalies over eastern Asia reverse polarity, while a pronounced precipitation deficit appears over Indochina. As  
 165 a result, the precipitation pattern associated with increased European SO<sub>2</sub> emissions closely resembles  
 166 observations and shows greater similarity than ALL across Asia. The aerosol-related precipitation response is also  
 167 robust across most of the ensemble members (Supplementary Fig. S4). For example, the ensemble-mean rainfall  
 168 trend over the core Indian region amounts to  $+0.33$  mm day<sup>-1</sup> over 55 years, with increases in 6 out of 8 ensemble  
 169 members. This indicates that European aerosols substantially contributed to the early 20<sup>th</sup>-century ASM rainfall  
 170 trends.

171

172 The observed and simulated 55-year rainfall trends over central-northern India are also compared with the  
 173 corresponding range of trends from the PI experiment (Supplementary Figs. S4 and S5). The trend from CRU is  
 174 outside the respective 90% confidence interval, while it is slightly below in GPCC. The trend from the ALL-  
 175 ensemble mean is within the corresponding 90% confidence interval ( $+0.19$  mm day<sup>-1</sup> over 55 years), although



176 five of its members exhibit positive trends that are markedly discernible from internal variability. The ensemble-  
 177 mean drying trend in the fixEU experiment exceeds the 90% confidence level. As a result, the ensemble-mean  
 178 trend associated with European aerosols (EU) is clearly distinguishable from internally-generated fluctuations,  
 179 even exceeding the 95% confidence level ( $+0.24 \text{ mm day}^{-1}$  over 55 years).

### 180 **3.2 Changes in the monsoon circulation**

181 Changes in precipitation across Asia are closely linked with variations in near-surface and atmospheric circulation  
 182 patterns (Fig. 2). The spatial correspondence between wet (dry) anomalies and regions of moisture flux  
 183 convergence (divergence) underscores the dominant role of circulation-induced moisture transport in shaping  
 184 monsoon precipitation trends (Fig. 2b). Over South Asia, a prominent anomalous anticyclone centred over  
 185 southern India and the western BoB characterises the low-tropospheric flow. Over East Asia and the western  
 186 Pacific, a zonal dipole emerges: an anomalous cyclone spans northern Indochina, southeastern China, and the  
 187 South China Sea, accompanied by an elongated anticyclone extending from central China to the western Pacific.

188  
 189 As Figure 2a shows, strong low-level easterlies across southern India oppose the climatological westerlies from  
 190 the Arabian Sea, leading to local rainfall deficits. Meanwhile, the climatological moisture-laden southwesterlies  
 191 are deflected northward over the northern Arabian Sea. Upon reaching central and northern India, this flow  
 192 converges with anomalous northeasterlies from northern Indochina and the northern BoB, enhancing rainfall (Fig.  
 193 2b). On the western flank of the anomalous Indo-Pakistan low, dry northerlies suppress precipitation over  
 194 Pakistan. Over East Asia, enhanced Pacific moisture transport into southern China and northeastern Indochina,  
 195 opposing the climatological southerlies linked to the western Pacific subtropical high, leads to regional wetting.  
 196 Return westerlies south of the anomalous Pacific low further reinforce the moisture flux from the BoB,  
 197 contributing to widespread wetting across the Bay and northwestern Indochina. In contrast, reduced southerly  
 198 moisture advection brings drying to southern Indonesia and northeastern China.

199  
 200 Figure 2c shows that the regional upper-tropospheric circulation also exhibits substantial changes, consistent with  
 201 the tropical balance among convective heating, ascent, and upper-level divergence (and vice versa). Over northern  
 202 India and the northern BoB, strong mid-tropospheric ascent coincides with rainfall enhancement, accompanied by  
 203 divergent outflow in the upper troposphere. One branch heads northeastward, converging and subsiding over  
 204 Burma and central China. Other branches are directed southwestward and southward, with corresponding mid-



205 tropospheric subsidence and surface anticyclones over southern India and the northern equatorial Maritime  
 206 Continent. A meridional system of divergent cells over East Asia and the western Pacific reflects the deep  
 207 convection and upper-tropospheric divergence centred near 20°N. The southern cell also converges and subsides  
 208 over the north equatorial Maritime Continent, aligning with the southern outflow from South Asia.

### 209 **3.3 Aerosol forcing over Europe**

210 To elucidate the generating mechanism, Figure 3a shows the widespread sulphate loading anomaly over Europe  
 211 resulting from enhanced emissions. Once emitted, aerosols are transported across and beyond the Continent.  
 212 Notably, aerosols spread southwestward towards northern Africa and the tropical Atlantic via the summertime  
 213 climatological circulation of the Azores high, and eastward over central Eurasia by the midlatitude climatological  
 214 westerlies, displacing the maximum loading and AOD (not shown) eastward of the emissions source.

215

216 Consistent with this transport, surface clear-sky downward shortwave radiation decreases across Europe, with  
 217 anomalies exceeding  $-3 \text{ W m}^{-2}$  over 55 years in regions of peak aerosol loading (Fig. 3b), accounting for  
 218 approximately 80% of the local reduction in the all-sky radiation (Supplementary Fig. S6). All-sky radiation  
 219 anomalies are larger (up to  $-5 \text{ W m}^{-2}$ ) due to increased cloudiness associated with circulation changes (see later).  
 220 As expected by the aerosol scattering effect, net shortwave differences between the top-of-atmosphere and surface  
 221 are minimal (not shown). Including longwave effects, the net radiative cooling at the model top reached about  $-2$   
 222  $\text{W m}^{-2}$  over central and eastern Europe (Supplementary Fig. S6).

223

224 Cloud droplet number concentration displays widespread positive anomalies over central and eastern Europe  
 225 concurrently with a negative, albeit weak, decrease in cloud top effective radius (Supplementary Fig. S6). These  
 226 changes are consistent with those expected by the cloud response to sulphate aerosols, assuming negligible  
 227 variations in water liquid content. The latter remains relatively unchanged or slightly enhanced due to anomalous  
 228 northwesterlies from the Atlantic (see below).

229

230 As a result of the aerosol-induced dimming, near-surface temperature shows anomalous cooling over central and  
 231 eastern Europe (Fig. 3c), and concurrently, the circulation adjusts thermodynamically, with marked anticyclonic  
 232 anomalies occurring at the surface. Interestingly, Fig. 3d shows that the largest cooling and the high-pressure core  
 233 are displaced east of the aerosol loading maximum, suggesting the combined influence of direct forcing,





234 feedbacks, and modulation by the climatological flow. For example, eastward aerosol transport and temperature  
 235 advection by the climatological westerlies contribute in concert to displacing the aerosol cooling to the east. The  
 236 associated northeasterly flow on the eastern flank of the surface anticyclone further reinforces the cooling over  
 237 eastern Europe. Note that the simulated eastward displacement of the anomalous anticyclone is consistent with  
 238 the pattern of observed sea-level pressure trends (Supplementary Fig. S7).

### 239 **3.4 Rossby wave propagation and remote teleconnections**

240 As shown in Figure 4, the regional signature of European aerosols extends to the mid and upper troposphere.  
 241 Streamfunction anomalies feature a (weak) equivalent-barotropic nature and a slight northwestward tilt with  
 242 height (not shown), consistent with the mature phase of an extratropical disturbance. At 300 hPa, anticyclonic  
 243 anomalies are seen over central Europe. This pattern forms part of a wave train signal extending across the  
 244 northern hemisphere, indicating a Rossby wave response to increased European aerosols and related upper-level  
 245 relative vorticity anomalies, which serve as the primary source of wave activity.

246

247 Upper-level meridional wind anomalies align with expectations from the streamfunction/geopotential height  
 248 pattern, revealing alternating cyclonic and anticyclonic centres (Fig. 4b). The wave activity flux (e.g., Takaya and  
 249 Nakamura 2001) highlights two eastward propagation branches. The main branch extends southeastward across  
 250 the Middle East to Pakistan and northwestern India, where it weakens while turning northeastward into eastern  
 251 China and converges over Japan. This flux follows the Asian jet stream, which acts as a Rossby waveguide. A  
 252 secondary, weaker high-latitude pathway is also evident: the wave flux points northeastward towards northern  
 253 Russia, crosses northern Eurasia, and then turns southeastward over the northwestern Pacific, ultimately  
 254 converging with the main pathway.

255

256 Mid-tropospheric ascent and descent anomalies accompany the wave train (Fig. 4b), consistent with the vorticity  
 257 balance (e.g., Rodwell and Hoskins 2001). For example, the anticyclonic anomaly over Afghanistan and Pakistan  
 258 induces southward flow and subsidence to its east, suppressing precipitation over Pakistan and the western Tibetan  
 259 Plateau. Conversely, over southern China, near-surface low-pressure anomalies, upward motion, and increased  
 260 precipitation are associated with northward flow. These results suggest that key upper-tropospheric action centres,  
 261 over the Middle East and southern China, initiate low-tropospheric circulation adjustments that generate the  
 262 anomalous rainfall pattern across Asia.



#### 263    **4 Discussion and concluding remarks**

264    The Asian summer monsoon hydroclimate underwent significant changes in the early 20<sup>th</sup> century, characterised  
 265    by a wetting trend over South Asia and a southern rainfall shift over East Asia. This study finds that increased  
 266    European anthropogenic sulphate aerosols played a key role in driving these observed monsoon changes. The  
 267    aerosol-induced cooling and large-scale anticyclonic anomaly over central/eastern Europe extend from the surface  
 268    to the upper troposphere. These anomalies trigger subsequent atmospheric circulation adjustments in the form of  
 269    an eastward propagating Rossby-wave train, which is central to realising the remote aerosol impact across Asia.

270

271    These findings shed new light on the drivers and mechanisms of monsoon multidecadal variability. While most  
 272    existing research has focused on recent monsoon changes, the early historical period remains unexplored.  
 273    Moreover, many prior studies have relied on long, equilibrium-type experiments to enhance the signal-to-noise  
 274    ratio, but these are less representative of the transient response to evolving aerosol emissions. An atmospheric  
 275    propagation pathway similar to the one identified here has been discussed in earlier literature, particularly in  
 276    relation to the downstream signature of the North Atlantic Oscillation (e.g., Watanabe 2004) and broader  
 277    teleconnections between Europe and East Asia (e.g., Lu et al. 2002; Enomoto et al., 2003), yet it has been largely  
 278    overlooked in the context of aerosol forcing (e.g., Wang et al., 2021b), which has instead typically emphasised  
 279    changes in the large-scale meridional temperature gradient across Eurasia as the dominant key mechanism.

280

281    Placing our study within the broader literature on remote aerosol-monsoon interactions underscores its relevance.  
 282    Cowan and Cai (2011) were among the first to identify the influence of non-Asian aerosols, primarily European  
 283    sulphate, in weakening the ASM over the 20<sup>th</sup> century by inducing widespread Eurasian cooling and thereby  
 284    reducing the meridional temperature gradient, which in turn weakens the southerly monsoon flow. Similarly, Guo  
 285    et al. (2015, 2016) linked widespread drying across Asia to increased global aerosol emissions, mainly from non-  
 286    Asian sources, and the subsequent modulation of the zonal-mean meridional temperature gradient. Focusing on  
 287    the fast, atmospheric-only equilibrium response to the removal of European aerosols, Dong et al. (2016) reported  
 288    a strengthening of the South Asian monsoon and a southern shift in East Asian rainfall, attributed to the  
 289    downstream advection of cooler, drier air from Europe to Asia and consequent weakening of the tropospheric  
 290    thermal gradient. Shawki et al. (2018) similarly found that removing European aerosol emissions strengthens,  
 291    albeit weakly, the South Asian monsoon and shifts the East Asian monsoon northward, via changes in the large-



292 scale temperature gradient and the interhemispheric heat and moisture transport. Liu et al. (2018) reported a slight  
 293 decrease in annual mean precipitation over Asia associated with increased European sulphate aerosols, driven by  
 294 the slow (ocean-mediated) component of the total response via inter-hemispheric heating redistribution. Similar  
 295 rainfall patterns were also shown by Westervelt et al. (2018). More recently, Wang et al. (2017) and Wang et al.  
 296 (2020) highlighted that non-local aerosol emissions are as influential as local ones in weakening the East Asian  
 297 summer monsoon, primarily through easterly advection of colder air across Eurasia and resulting change in  
 298 meridional heat transport, in agreement with Dong et al. (2016).

299

300 An enhanced meridional temperature gradient between central Eurasia and the IO is a well-known contributor to  
 301 stronger monsoon precipitation over South Asia (e.g., Meehl and Arblaster, 2002). Indeed, this has been identified,  
 302 for example, as one of the elements contributing to enhanced future monsoon precipitation by the end of the 21<sup>st</sup>  
 303 century (e.g., Meehl et al., 2024). This outcome, however, is not borne out in our study, as the mid and high  
 304 troposphere temperature averaged over the 60°-100°E sector displays enhanced cooling compared to the north-  
 305 equatorial IO, resulting in a weaker meridional temperature gradient (not shown). This discrepancy indicates that  
 306 the aerosol-induced regional monsoon circulation and precipitation variations over South Asia cannot be explained  
 307 by broad-scale sector-mean temperature changes. On the contrary, the anomalous temperature pattern over Eurasia  
 308 displays a close relationship with that induced by the anomalies in atmospheric advection, especially in the  
 309 meridional direction, in turn associated with the upper-tropospheric wave train.

310

311 This dynamical pathway and the critical role of large-scale remotely driven atmospheric dynamical changes finds  
 312 support in Bollasina et al. (2014). Although secondary to regional emissions in explaining the recent monsoon  
 313 rainfall decline, extratropical aerosols were nonetheless shown to induce widespread temperature and wind  
 314 anomalies across Asia, revealing the complex interplay between aerosol forcing, precipitation, and circulation  
 315 changes. Undorf et al. (2018a, b) also highlighted the importance of midlatitude aerosol forcing in explaining the  
 316 observed weakening of the South Asian monsoon through the mid-1970s, underscoring the key role of Eurasian-  
 317 scale dynamical adjustments.

318

319 An important question is whether Indian Ocean (IO) SSTs also influenced the monsoon. The ALL ensemble,  
 320 consistent with the overall performance of CMIP5/6 models (e.g., Roxy et al., 2014), exhibits widespread and



321 relatively homogeneous warming across the basin. In contrast, aerosol-induced SST trends, albeit weak, show  
 322 warming over the western equatorial IO and cooling over the subequatorial regions (Supplementary Fig. S8). This  
 323 cross-equatorial dipole in SST trends is also evident, and more pronounced, in observations (e.g., Fig. 3 in  
 324 Goswami et al., 2023), which suggests an aerosol contribution to the IO warming pattern. Further analysis of the  
 325 EU ensemble (not shown), shows that SST anomalies are largely anticorrelated with evaporation: reduced  
 326 evaporation dominates the western and equatorial IO, while increases are seen in the south. Concurrently,  
 327 anomalous near-surface divergent easterlies across the north-equatorial IO oppose the climatological (south)  
 328 westerlies, reducing evaporation and upwelling, which contribute to warming the SSTs. These patterns are similar  
 329 to those associated with the Indian summer monsoon multi-decadal variability during the 20<sup>th</sup> century (Goswami  
 330 et al., 2023). Also, the 55-year SST pattern resembles 20<sup>th</sup>-century-long changes, although the latter exhibits  
 331 weaker anomalies and a less pronounced cooling (e.g., Rao et al., 2012; Roxy et al., 2014). Uncertainties remain  
 332 in identifying the causes of the persistent western IO warming due to strong feedbacks between oceanic anomalies,  
 333 atmospheric circulation, and convection (e.g., Rao et al., 2012; Swapna et al., 2014). While our findings highlight  
 334 the role of remotely-forced wind anomalies, other mechanisms may also contribute. While SST anomalies and  
 335 rainfall are anticorrelated in the long term, this relationship reverses in the early 20<sup>th</sup> century (Fig. 3 in Roxy et  
 336 al., 2015), aligning with our findings.

337  
 338 Our results have important implications. They suggest that non-local anthropogenic aerosols have contributed  
 339 significantly to shaping monsoon variability even during the early historical period. This is particularly relevant  
 340 for understanding regional-scale impacts of anthropogenic forcing, which remain uncertain due to the spatial  
 341 heterogeneity of emissions and their diverse climate effects. Importantly, under the current continued decrease in  
 342 European aerosol emissions, assuming an opposite ASM response to the one described above, remotely-driven  
 343 precipitation anomalies may significantly modulate, if not partially offset, the response to Asian aerosol emission  
 344 changes (already declining or expected to do so in the future; e.g., Lund et al., 2019; Xiang et al. 2023). For  
 345 example, assuming linearity in the combined responses, the abatement of EU sulphate aerosols would lead to a  
 346 weaker monsoon over most of South Asia, and India in particular, which is opposite to the expected wetting  
 347 associated with decreased sulphate aerosols over both South and East Asia (e.g., Bartlett et al., 2018). Conversely,  
 348 EU aerosol reductions would contribute to further amplify the reversed SFND pattern over China brought about  
 349 by decreased East Asian aerosol alone (e.g., Dong et al., 2016), resulting, for example, in enhanced drying over



southeastern China. While the future monsoon response to the projected decline in worldwide aerosol emissions will most likely result from non-linear interactions among the different aerosol source regions, the above picture illustrates the complex interplay among local and remote aerosols and the need for a consistent and coordinated modelling and analysis approach (e.g., Wilcox et al., 2023).

354

While our analysis emphasises the central role of European aerosols, other remote emissions (e.g., from North America) and external forcings (e.g., greenhouse gases) may have also played a role. Our conclusions are based on ensemble experiments comprising eight members each, consistent with the minimum number typically recommended for detecting forced multi-decadal signals (e.g., Deser et al., 2012). However, internal variability cannot be ruled out, and studies have, for example, discussed the association of Atlantic slow-frequency variability with the ISM multi-decadal mode (e.g., Rajesh and Goswami, 2020). In this context, the use of large single-forcing ensembles (e.g., Smith et al., 2022; Simpson et al., 2023) offers a promising approach to disentangling the individual contributions of greenhouse gases, anthropogenic aerosols and other external drivers. Furthermore, our findings are based on a single climate model and therefore depend on its representation of aerosol-cloud-radiation and circulation interactions. Given the well-known uncertainties in aerosol forcing and its climatic effects, the response may differ across models and from real-world observations. For example, CESM1 is known to exhibit a relatively strong aerosol effective radiative forcing (Zelinka et al., 2014; 2023), which may result in a stronger climate response to aerosol perturbations than seen in other models.

368

**Acknowledgements.** MAB acknowledges support from the Natural Environment Research Council (NE/N006038/1) and the Research Council of Norway (grant no. 324182; CATHY).

371

**Data availability.** GPCC data are retrieved from <https://psl.noaa.gov/data/gridded/data.gpcc.html>, CRU data from <https://crudata.uea.ac.uk/cru/data/hrg/>, and UDEL data from [https://psl.noaa.gov/data/gridded/data.UDEL\\_AirT\\_Precip.html](https://psl.noaa.gov/data/gridded/data.UDEL_AirT_Precip.html). The ERA5 data are obtained at <https://cds.climate.copernicus.eu/datasets/reanalysis-era5-pressure-levels-monthly-means>. HadISST data are available from <https://www.metoffice.gov.uk/hadobs/hadisst/>, while the HadSLP2 dataset is accessed from <https://www.metoffice.gov.uk/hadobs/hadslp2/>. The CESM model data used in this study are available from MAB upon request.

379



380    **Author contribution.** WS and MAB designed the study. WS performed the analysis and completed the first draft  
381    of the manuscript. WS and MAB discussed the results, WA, MAB, and IC edited the manuscript. GW and YL  
382    provided suggestions on the analysis and interpretation of the results.

383

384    **Competing interests.** The authors have no competing interests to declare.

385



## 386 References

- 387 Allan, R., and Ansell, T.: A New Globally Complete Monthly Historical Gridded Mean Sea Level Pressure Dataset  
 388 (HadSLP2): 1850–2004, *J. Climate*, 19, <https://doi.org/10.1175/JCLI3937.1>, 2006.
- 389 Andrews, T., and Forster, P.M.: Energy budget constraints on historical radiative forcing, *Nat. Clim. Chang.* 10,  
 390 <https://doi.org/10.1038/s41558-020-0696-1>, 2020.
- 391 Bartlett, R. E., Bollasina, M. A., Booth, B. B. B. et al.: Do differences in future sulfate emission pathways matter  
 392 for near-term climate? A case study for the Asian monsoon, *Clim. Dynam.*, 50, [https://doi.org/10.1007/s00382-](https://doi.org/10.1007/s00382-017-3726-6)  
 393 [017-3726-6](https://doi.org/10.1007/s00382-017-3726-6), 2018.
- 394 Bellouin, N., et al.: Bounding aerosol radiative forcing of climate change, *Rev. Geophys.*, 58,  
 395 <https://doi.org/10.1029/2019RG000660>, 2020.
- 396 Bollasina, M.A, Ming, Y, Ramaswamy, V.: Anthropogenic aerosols and the weakening of the South Asian summer  
 397 monsoon, *Science*, 334, <https://doi.org/10.1126/science.1204994>, 2011.
- 398 Bollasina, M. A., Ming, Y., Ramaswamy, V., Schwarzkopf, M. D., and Naik, V.: Contribution of local and remote  
 399 anthropogenic aerosols to the twentieth century weakening of the South Asian monsoon, *Geophys. Res. Lett.*,  
 400 41, <https://doi.org/10.1002/2013GL058183>, 2014.
- 401 Boucher, O., Randall, D., Artaxo, P., Bretherton, C., Feingold, G., Forster, P., Kerminen, V.-M., Kondo, Y., Liao,  
 402 H., Lohmann, U., Rasch, P., Satheesh, S., Sherwood, S., Stevens, B., and Zhang, X.: Clouds and aerosols, in  
 403 *Climate change 2013: The physical science basis. Contribution of Working Group I to the Fifth Assessment*  
 404 *Report of the Intergovernmental Panel on Climate Change*, edited by Stocker T., Qin D., Plattner G.-K., Tignor  
 405 M., Allen S., Boschung J., Nauels A., Xia Y., Bex V., and Midgley P., chap. 7, pp. 571–658, Cambridge  
 406 University Press, Cambridge, United Kingdom and New York, NY, USA,  
 407 <https://10.1017/CBO9781107415324.016>, 2013.
- 408 Cowan, T. and Cai, W.: The impact of Asian and non-Asian anthropogenic aerosols on 20th century Asian summer  
 409 monsoon, *Geophys. Res. Lett.*, 38, <https://doi.org/10.1029/2011GL047268>, 2011.
- 410 Deser, C., Phillips, A., Bourdette, V., et al.: Uncertainty in climate change projections: the role of internal  
 411 variability, *Clim. Dynam.*, 38, <https://doi.org/10.1007/s00382-010-0977-x>, 2012.
- 412 Dong, B., Sutton, R. T., Highwood, E. J., and Wilcox, L. J.: Preferred response of the East Asian summer monsoon  
 413 to local and non-local anthropogenic sulphur dioxide emissions, *Clim. Dynam.*, 46,  
 414 <https://doi.org/10.1007/s00382-015-2671-5>, 2016.



- 415 Dong, B., Wilcox, L.J., Highwood, E.J., and Sutton, R. T.: Impacts of recent decadal changes in Asian aerosols on  
 416 the East Asian summer monsoon: roles of aerosol–radiation and aerosol–cloud interactions, *Clim. Dynam.*,  
 417 53, <https://doi.org/10.1007/s00382-019-04698-0>, 2019.
- 418 Enomoto, T., Hoskins, B.J., and Matsuda, Y.: The formation mechanism of the Bonin high in August, *Q. J. Roy.*  
 419 *Meteor. Soc.*, 129, <https://doi.org/10.1256/qj.01.211>, 2003.
- 420 Gadgil, S., and Rupa Kumar, K.: The Asian monsoon — agriculture and economy. In: *The Asian Monsoon*.  
 421 Springer Praxis Books. Springer, Berlin, Heidelberg. [https://doi.org/10.1007/3-540-37722-0\\_18](https://doi.org/10.1007/3-540-37722-0_18), 2006.
- 422 Ghan, S. J., Liu, X., Easter, R. C., Zaveri, R., Rasch, P. J., et al.: Toward a minimal representation of aerosols in  
 423 climate models: Comparative decomposition of aerosol direct, semidirect, and indirect radiative forcing, *J.*  
 424 *Climate*, 25, <https://doi.org/10.1175/JCLI-D-11-00650.1>, 2012.
- 425 Goswami, D. J., Ashok, K., and Goswami, B. N.: Local ocean–atmosphere interaction in Indian summer monsoon  
 426 multi-decadal variability, *Clim. Dynam.*, 60, <https://doi.org/10.1007/s00382-022-06377-z>, 2023.
- 427 Guo, L., Highwood, E. J., Shaffrey, L. C., and Turner, A. G.: The effect of regional changes in anthropogenic  
 428 aerosols on rainfall of the East Asian summer monsoon, *Atmos. Chem. Phys.*, 13, [https://doi.org/10.5194/acp-](https://doi.org/10.5194/acp-13-1521-2013)  
 429 [13-1521-2013](https://doi.org/10.5194/acp-13-1521-2013), 2013.
- 430 Guo, L., Turner, A. G., and Highwood, E. J.: Impacts of 20<sup>th</sup> century aerosol emissions on the South Asian  
 431 monsoon in the CMIP5 models, *Atmos. Chem. Phys.*, 15, <https://doi.org/10.5194/acp-15-6367-2015>, 2015.
- 432 Harris, I., Jones, P.D., Osborn, T.J. and Lister, D.H.: Updated high-resolution grids of monthly climatic  
 433 observations – the CRU TS3.10 Dataset, *Int. J. Climatol.*, 34, <https://doi.org/10.1002/joc.3711>, 2014.
- 434 He, L., Zhou, T., and Chen, X.: South Asian summer rainfall from CMIP3 to CMIP6 models: biases and  
 435 improvements, *Clim. Dynam.*, 61, <https://doi.org/10.1007/s00382-022-06542-4>, 2023.
- 436 Hegerl G.C., Bronnimann S., et al.: Causes of climate change over the historical record, *Environ. Res. Lett.*, 14,  
 437 <https://doi.org/10.1088/1748-9326/ab4557>, 2019.
- 438 Hersbach, H., Bell, B., Berrisford, P., et al.: The ERA5 global reanalysis. *Q. J. Roy. Meteor. Soc.*, 146,  
 439 <https://doi.org/10.1002/qj.3803>, 2020.
- 440 Hoesly, R.M., et al.: Historical (1750–2014) anthropogenic emissions of reactive gases and aerosols from the  
 441 Community Emissions Data System (CEDS), *Geosci. Model Dev.*, 11, [https://doi.org/10.5194/gmd-11-369-](https://doi.org/10.5194/gmd-11-369-2018)  
 442 [2018](https://doi.org/10.5194/gmd-11-369-2018), 2018.
- 443 Huang, X., and Coauthors: The recent decline and recovery of Indian summer monsoon rainfall: relative roles of





- 444 external forcing and internal variability, *J. Climate*, 33, <https://doi.org/10.1175/JCLI-D-19-0833.1>, 2020.
- 445 Hurrell, J. W., Holland, M. M., Gent, P. R., Ghan, S., Kay, J. E., et al.: The Community Earth System Model, *Bull.*
- 446 *Amer. Met. Soc.*, 94, <https://doi.org/10.1175/BAMS-D-12-00121.1>, 2013.
- 447 Koffi, B., Dentener, F., Janssens-Maenhout, G., Guizzardi, D., Crippa, M., et al.: Hemispheric transport air
- 448 pollution (HTAP): Specification of the HTAP2 experiments ensuring harmonized modelling (Tech. rep.)
- 449 Luxembourg: Joint Research Centre JRC. <https://doi.org/10.2788/725244>, 2016.
- 450 Lau, W.K.M.: The aerosol-monsoon climate system of Asia: A new paradigm, *J. Meteor. Res.*, 30,
- 451 <https://doi.org/10.1007/s13351-015-5999-1>, 2016.
- 452 Li, X., Li, Q., Ding, Y., Yang, S., et al.: Possible influence of the interdecadal variation of the extratropical southern
- 453 Indian Ocean SST on East Asian summer monsoon precipitation, *Atmos. Res.*, 288,
- 454 <https://doi.org/10.1016/j.atmosres.2023.106721>, 2023.
- 455 Li, X., Ting, M., Li, C., and Henderson, N.: Mechanisms of Asian summer monsoon changes in response to
- 456 anthropogenic forcing in CMIP5 models, *J. Climate*, 28, <https://doi.org/10.1175/JCLI-D-14-00559.1>, 2015.
- 457 Li, Z., et al.: Aerosol and monsoon climate interactions over Asia, *Rev. Geophys.*, 54,
- 458 <https://doi.org/10.1002/2015RG000500>, 2016.
- 459 Li, J., Carlson, B.E., Yung, Y.L., et al.: Scattering and absorbing aerosols in the climate system, *Nat. Rev. Earth*
- 460 *Environ.*, 3, <https://doi.org/10.1038/s43017-022-00296-7>, 2022.
- 461 Liu, L., Shawki, D., Voulgarakis, A., Kasoar, M., Samset, B. H., et al.: A PDRMIP Multimodel study on the
- 462 impacts of regional aerosol forcings on global and regional precipitation, *J. Climate*, 31,
- 463 <https://doi.org/10.1175/JCLI-D-17-0439.1>, 2018.
- 464 Liu, Y., Cai, W., Sun, C., Song, H., Cobb, K. M., et al.: Anthropogenic aerosols cause recent pronounced
- 465 weakening of Asian summer monsoon relative to last four centuries, *Geophys. Res. Lett.*, 46, 5469–5479,
- 466 <https://doi.org/10.1029/2019GL082497>, 2019.
- 467 Liu, Z., Bollasina, M. A., and Wilcox, L. J.: Impact of Asian aerosols on the summer monsoon strongly modulated
- 468 by regional precipitation biases, *Atmos. Chem. Phys.*, 24, 7227–7252, [https://doi.org/10.5194/acp-24-7227-](https://doi.org/10.5194/acp-24-7227-2024)
- 469 [2024](https://doi.org/10.5194/acp-24-7227-2024), 2024.
- 470 Lu, R.-Y., Oh, J.H., and Kim, B.J.: A teleconnection pattern in upper-level meridional wind over the North African
- 471 and Eurasian continent in summer, *Tellus A*, 54, <https://doi.org/10.3402/tellusa.v54i1.12122>, 2002.
- 472 Lund, M. T., Myhre, G., and Samset, B. H.: Anthropogenic aerosol forcing under the Shared Socioeconomic



- 473 Pathways, Atmos. Chem. Phys., 19, <https://doi.org/10.5194/acp-19-13827-2019>, 2019.
- 474 Meehl, G. A., and Arblaster, J. M.: GCM sensitivity experiments for the Indian monsoon and tropospheric biennial  
 475 oscillation transition conditions, J. Climate, 15, [https://doi.org/10.1175/1520-0442\(2002\)015<0923:imgset>2.0.co;2](https://doi.org/10.1175/1520-0442(2002)015<0923:imgset>2.0.co;2), 2002.
- 476
- 477 Meehl, G.A., Shields, C., Arblaster, J.M., Annamalai, H., and Neale, R.: Intraseasonal, seasonal, and interannual  
 478 characteristics of regional monsoon simulations in CESM2, J. Adv. Model. Earth Sys., 12,  
 479 <https://doi.org/10.1029/2019MS001962>, 2020.
- 480 Meehl, G. A., Shields, C. A., Arblaster, J. M., Fasullo, J., Rosenbloom, N., Hu, A., et al.: Processes that contribute  
 481 to future South Asian monsoon differences in E3SMv2 and CESM2, Geophys. Res. Lett., 51,  
 482 <https://doi.org/10.1029/2024GL109056>, 2024.
- 483 Neale, R. B., Gettelman, A., Park, S., Chen, C.-C., Lauritzen, P. H., et al.: Description of the NCAR Community  
 484 Atmosphere Model (CAM 5.0), NCAR technical note, NCAR/TN-48, 274.  
 485 <https://doi.org/10.5065/D6N877R0>, 2012.
- 486 Persad, G., Samset, B.H., Wilcox, L.J., Allen, R.J., Bollasina, M.A., et al.: Rapidly evolving aerosol emissions are  
 487 a dangerous omission from near-term climate risk assessments, Environ. Res. Climate, 2,  
 488 <https://doi.org/10.1088/2752-5295/acd6af>, 2023.
- 489 Preethi, B., Mujumdar, M., Kripalani, R.H. et al.: Recent trends and tele-connections among South and East Asian  
 490 summer monsoons in a warming environment, Clim. Dynam., 48, [https://doi.org/10.1007/s00382-016-3218-](https://doi.org/10.1007/s00382-016-3218-0)  
 491 [0](https://doi.org/10.1007/s00382-016-3218-0), 2017.
- 492 Rajesh, P. V., and Goswami, B. N.: Four-dimensional structure and sub-seasonal regulation of the Indian summer  
 493 monsoon multi-decadal mode, Clim. Dynam., 55, <https://doi.org/10.1007/s00382-020-05407-y>, 2020.
- 494 Rao, S.A., Dhakate, A.R., Saha, S.K. et al.: Why is Indian Ocean warming consistently?, Climatic Change, 110,  
 495 <https://doi.org/10.1007/s10584-011-0121-x>, 2012.
- 496 Rayner, N. A., Parker, D. E., Horton, E. B., Folland, C. K., Alexander, L. V., Rowell, D. P., Kent, E. C., and  
 497 Kaplan, A.: Global analyses of sea surface temperature, sea ice, and night marine air temperature since the late  
 498 nineteenth century, J. Geophys. Res., 108, <https://doi.org/10.1029/2002JD002670>, 2003.
- 499 Rodwell, M. J., and Hoskins, B. J.: Subtropical anticyclones and summer monsoons, J. Climate, 14,  
 500 [https://doi.org/10.1175/1520-0442\(2001\)014<3192:SAASM>2.0.CO;2](https://doi.org/10.1175/1520-0442(2001)014<3192:SAASM>2.0.CO;2), 2001.
- 501 Roxy, M. K., Ritika, K., Terray, P., and Masson, S.: The curious case of Indian Ocean warming. J. Climate, 27,



- 502 <https://doi.org/10.1175/JCLI-D-14-00471.1>, 2014.
- 503 Roxy, M., Ritika, K., Terray, P. et al.: Drying of Indian subcontinent by rapid Indian Ocean warming and a  
 504 weakening land-sea thermal gradient, *Nat. Commun.*, 6, <https://doi.org/10.1038/ncomms8423>, 2015.
- 505 Saha, A., and Ghosh, S.: Can the weakening of the Indian Monsoon be attributed to anthropogenic aerosols?  
 506 *Environ. Res. Commun.*, 1, <https://doi.org/10.1088/2515-7620/ab2c65>, 2019.
- 507 Salzmann, M., Weser, H., Cherian, R.: Robust response of Asian summer monsoon to anthropogenic aerosols in  
 508 CMIP5 models, *J. Geophys. Res. Atmos.*, 119, <https://doi.org/10.1002/2014JD021783>, 2014.
- 509 Salzmann, M., and Cherian, R.: On the enhancement of the Indian summer monsoon drying by Pacific  
 510 multidecadal variability during the latter half of the twentieth century, *J. Geophys. Res. Atmos.*, 120,  
 511 <https://doi.org/10.1002/2015JD023313>, 2015.
- 512 Samset, B. H., et al.: Climate impacts from a removal of anthropogenic aerosol emissions. *Geophys. Res. Lett.*,  
 513 45, <https://doi.org/10.1002/2017GL076079>, 2018.
- 514 Samset, B.H., Lund, M.T., Bollasina, M., et al.: Emerging Asian aerosol patterns. *Nat. Geosci.*, 12,  
 515 <https://doi.org/10.1038/s41561-019-0424-5>, 2019.
- 516 Schneider, U., Becker, A., Finger, P. et al.: GPCC's new land surface precipitation climatology based on quality-  
 517 controlled in situ data and its role in quantifying the global water cycle, *Theor. Appl. Climatol.*, 115,  
 518 <https://doi.org/10.1007/s00704-013-0860-x>, 2014,
- 519 Shao, Z., Wang, H., Geng, Y.F., et al.: East Asian summer monsoon response to anthropogenic aerosols  
 520 redistribution: contrasting 1950–1980 and 1980–2010 to understand the role of non-Asian forcing, *Clim.*  
 521 *Dynam.*, 62, <https://doi.org/10.1007/s00382-023-07016-x>, 2024.
- 522 Shawki, D., Voulgarakis, A., Chakraborty, A., Kassoar, M., and Srinivasan, J.: The South Asian monsoon response  
 523 to remote aerosols: Global and regional mechanisms, *J. Geophys. Res.*, 123,  
 524 <https://doi.org/10.1029/2018JD028623>, 2018.
- 525 Simpson, I. R., and Coauthors: The CESM2 single-forcing large ensemble and comparison to CESM1:  
 526 implications for experimental design. *J. Climate*, 36, <https://doi.org/10.1175/JCLI-D-22-0666.1>, 2023.
- 527 Smith, S. J., van Aardenne, J., Klimont, Z., Andres, R. J., Volke, A., and Delgado Arias, S.: Anthropogenic sulfur  
 528 dioxide emissions: 1850–2005, *Atmos. Chem. Phys.*, 11, <https://doi.org/10.5194/acp-11-1101-2011>, 2011.
- 529 Smith, D., Gillett, N. P., Simpson, I. R., Athanasiadis, P. J., Baehr, J., Bethke, I., et al.: Attribution of multi-annual  
 530 to decadal changes in the climate system: The large ensemble single forcing model intercomparison project



- 531 (LESFMIP), *Front. Clim.*, 4, <https://doi.org/10.3389/fclim.2022.955414>, 2022.
- 532 Song, F., Zhou, T., and Qian, Y.: Responses of East Asian summer monsoon to natural and anthropogenic forcings  
 533 in the 17 latest CMIP5 models, *Geophys. Res. Lett.*, 41, <https://doi.org/10.1002/2013GL058705>, 2014.
- 534 Stier, P., van den Heever, S.C., Christensen, M.W., et al.: Multifaceted aerosol effects on precipitation, *Nat.*  
 535 *Geosci.*, 17, <https://doi.org/10.1038/s41561-024-01482-6>, 2024.
- 536 Swapna, P., Krishnan, R., and Wallace, J.M.: Indian Ocean and monsoon coupled interactions in a warming  
 537 environment, *Clim. Dynam.*, 42, <https://doi.org/10.1007/s00382-013-1787-8>, 2014.
- 538 Szopa, S., et al.: Short-Lived Climate Forcers. In *Climate Change 2021: The Physical Science Basis. Contribution*  
 539 *of Working Group I to the Sixth Assessment Report of the Intergovernmental Panel on Climate Change*  
 540 [Masson-Delmotte, V., P. Zhai, A. Pirani, S.L. Connors, C. Péan, S. Berger, N. Caud, Y. Chen, L. Goldfarb,  
 541 M.I. Gomis, M. Huang, K. Leitzell, E. Lonnoy, J.B.R. Matthews, T.K. Maycock, T. Waterfield, O. Yelekçi, R.  
 542 Yu, and B. Zhou (eds.)]. Cambridge University Press, Cambridge, United Kingdom and New York, NY, USA,  
 543 pp. 817–922, <https://doi.org/10.1017/9781009157896.008>, 2021.
- 544 Takaya, K., and Nakamura, H.: A formulation of a phase-independent wave-activity flux for stationary and  
 545 migratory quasigeostrophic eddies on a zonally varying basic flow, *J. Atmos. Sci.*, 58,  
 546 [https://doi.org/10.1175/1520-0469\(2001\)058<0608:AFOAPI>2.0.CO;2](https://doi.org/10.1175/1520-0469(2001)058<0608:AFOAPI>2.0.CO;2), 2001.
- 547 Turner, A., and Annamalai, H.: Climate change and the South Asian summer monsoon, *Nature Clim. Change* 2,  
 548 <https://doi.org/10.1038/nclimate1495>, 2012
- 549 Undorf, S., Bollasina, M., Booth, B., and Hegerl, G.: Contrasting the effects of the 1850-1975 increase in sulphate  
 550 aerosols from North America and Europe on the Atlantic in the CESM, *Geophys. Res. Lett.*, 45,  
 551 <https://doi.org/10.1029/2018GL079970>, 2018.
- 552 Undorf, S., Polson, D., Bollasina, M. A., Ming, Y., Schurer, A., and Hegerl, G. C.: Detectable impact of local and  
 553 remote anthropogenic aerosols on the 20th century changes of West African and South Asian monsoon  
 554 precipitation, *J. Geophys. Res.*, 123, <https://doi.org/10.1029/2017JD027711>, 2018.
- 555 Wang, Q., Wang, Z., and Zhang, H.: Impact of anthropogenic aerosols from global, East Asian, and non-East  
 556 Asian sources on East Asian summer monsoon system, *Atmos. Res.*, 183,  
 557 <https://doi.org/10.1016/j.atmosres.2016.08.023>, 2017.
- 558 Wang, B., and Coauthors: Toward predicting changes in the land monsoon rainfall a decade in advance. *J. Climate*,  
 559 31, <https://doi.org/10.1175/JCLI-D-17-0521.1>, 2018.



- 560 Wang, Z., Mu, J., Yang, M., and Yu, X.: Reexamining the mechanisms of East Asian summer monsoon changes  
 561 in response to non–East Asian anthropogenic aerosol forcing. *J. Climate*, 33, [https://doi.org/10.1175/JCLI-D-](https://doi.org/10.1175/JCLI-D-19-0550.1)  
 562 [19-0550.1](https://doi.org/10.1175/JCLI-D-19-0550.1), 2020.
- 563 Wang, Z., Lin, L., Xu, Y., et al.: Incorrect Asian aerosols affecting the attribution and projection of regional climate  
 564 change in CMIP6 models, *npj Clim. Atmos. Sci.*, 4, <https://doi.org/10.1038/s41612-020-00159-2>, 2021.
- 565 Wang, Z., Feng, J., Diao, C., Li, Y., Lin, L., and Xu, Y.: Reduction in European anthropogenic aerosols and the  
 566 weather conditions conducive to PM<sub>2.5</sub> pollution in North China: a potential global teleconnection pathway,  
 567 *Environ. Res. Lett.*, 16, <https://doi.org/10.1088/1748-9326/ac269d>, 2021.
- 568 Watanabe, M.: Asian jet waveguide and a downstream extension of the North Atlantic Oscillation, *J. Climate*, 17,  
 569 <https://doi.org/10.1175/JCLI-3228.1>, 2004.
- 570 Westervelt, D. M., Conley, A. J., Fiore, A. M., Lamarque, J.-F., Shindell, D. T., Previdi, M., Mascioli, N. R.,  
 571 Faluvegi, G., Correa, G., and Horowitz, L. W.: Connecting regional aerosol emissions reductions to local and  
 572 remote precipitation responses, *Atmos. Chem. Phys.*, 18, 12461–12475, [https://doi.org/10.5194/acp-18-](https://doi.org/10.5194/acp-18-12461-2018)  
 573 [12461-2018](https://doi.org/10.5194/acp-18-12461-2018), 2018.
- 574 Wilcox, L. J., Allen, R. J., Samset, B. H., Bollasina, M. A., et al.: The Regional Aerosol Model Intercomparison  
 575 Project (RAMIP), *Geosci. Model Dev.*, 16, <https://doi.org/10.5194/gmd-16-4451-2023>, 2023.
- 576 Wilcox L. J., Liu, Z., Samset, B. H., et al.: Accelerated increases in global and Asian summer monsoon  
 577 precipitation from future aerosol reductions, *Atmos. Chem. Phys.*, 20, [https://doi.org/10.5194/acp-20-11955-](https://doi.org/10.5194/acp-20-11955-2020)  
 578 [2020](https://doi.org/10.5194/acp-20-11955-2020), 2020.
- 579 Willmott, C. J., and Matsuura, K.: Smart interpolation of annually averaged air temperature in the United States,  
 580 *J. Appl. Meteor. Climatol.*, 34, [https://doi.org/10.1175/1520-0450\(1995\)034<2577:SIOAAA>2.0.CO;2](https://doi.org/10.1175/1520-0450(1995)034<2577:SIOAAA>2.0.CO;2),  
 581 1995.
- 582 Wu, G. X., Li, Z. Q., Fu, C. B., Zhang, X. Y., Zhang, R. Y., Zhang, R. H., et al.: Advances in studying interactions  
 583 between aerosols and monsoon in China. *Science China Earth Sciences*, 59, [https://doi.org/10.1007/s11430-](https://doi.org/10.1007/s11430-015-5198-z)  
 584 [015-5198-z](https://doi.org/10.1007/s11430-015-5198-z), 2016.
- 585 Xiang, B., Xie, S. P., Kang, S. M. et al.: An emerging Asian aerosol dipole pattern reshapes the Asian summer  
 586 monsoon and exacerbates northern hemisphere warming, *npj Clim. Atmos. Sci.*, 6,  
 587 <https://doi.org/10.1038/s41612-023-00400-8>, 2023.
- 588 Xie, P., and Arkin, P. A.: Global precipitation: A 17-Year monthly analysis based on gauge observations, satellite



589 estimates, and numerical model outputs, Bull. Amer. Meteor. Soc., 78, <https://doi.org/10.1175/1520->  
590 [0477\(1997\)078<2539:GPAYMA>2.0.CO;2](https://doi.org/10.1175/1520-0477(1997)078<2539:GPAYMA>2.0.CO;2), 1997.

591 Zelinka, M. D., Andrews, T., Forster, P. M., and Taylor, K. E.: Quantifying components of aerosol-cloud-radiation  
592 interactions in climate models, J. Geophys. Res. Atmos., 119, <https://doi.org/10.1002/2014JD021710>, 2014.

593 Zelinka, M. D., Smith, C. J., Qin, Y., and Taylor, K. E.: Comparison of methods to estimate aerosol effective  
594 radiative forcings in climate models, Atmos. Chem. Phys., 23, <https://doi.org/10.5194/acp-23-8879-2023>,  
595 2023.

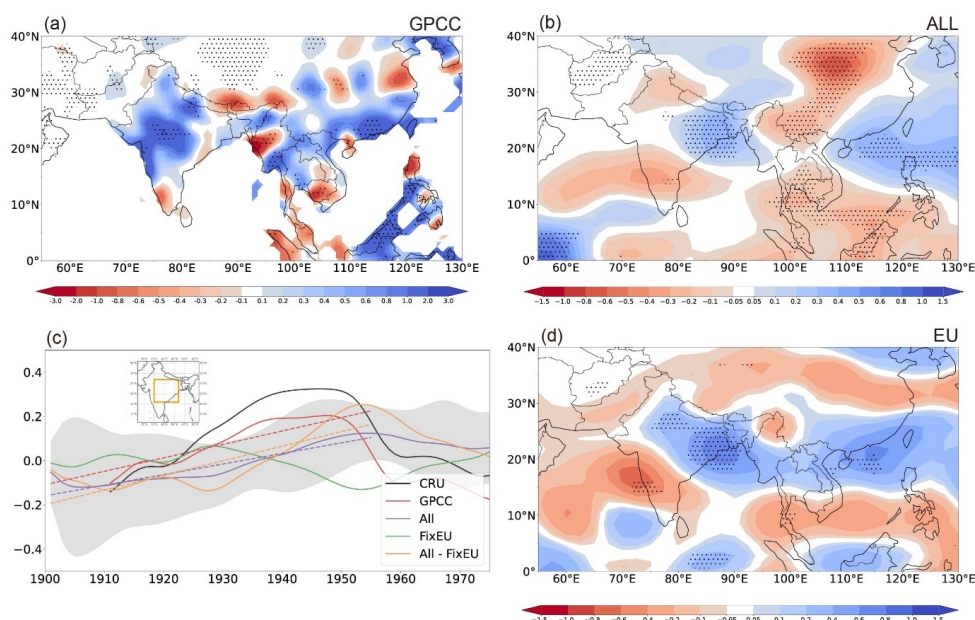
596 Zhang, L., and Zhou, T.: An assessment of monsoon precipitation changes during 1901–2001. Clim. Dynam., 37,  
597 <https://doi.org/10.1007/s00382-011-0993-5>, 2011.

598



## Figures

600



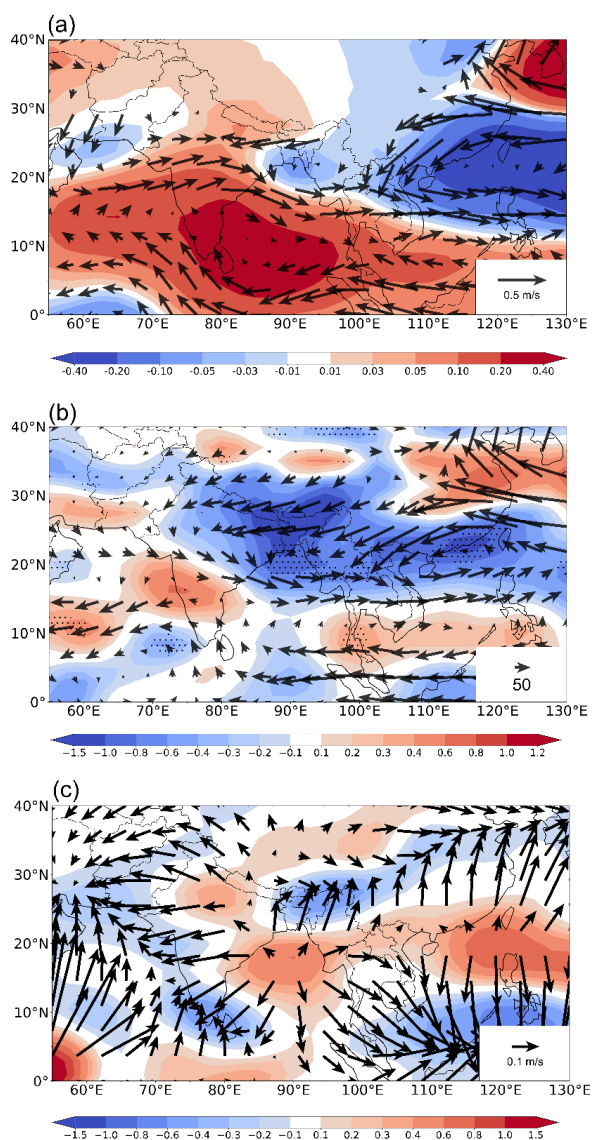
601

602

603 **Figure 1.** (a)-(b): Spatial patterns of the 1901-1955 linear trends of JJA precipitation ( $\text{mm day}^{-1} (55 \text{ years})^{-1}$ ) for  
 604 (a) GPCC, (b) the all-forcing ensemble (ALL), and (d) the difference between ALL and the all-forcing experiment  
 605 with fixed preindustrial aerosol emissions over Europe (fixEU), representing the impact of EU aerosols. The black  
 606 dots mark the grid points for which the trend exceeds the 90% significance level according to the two-tailed  
 607 Student's t-test. (c): Time series of area-averaged JJA precipitation anomalies ( $\text{mm day}^{-1}$ ; deviations from the  
 608 1901-2000 climatology) over central-northern India (land-only points within 75°–87°E, 16°–27°N; area shown in  
 609 inset map) smoothed with 11-year running means to highlight low-frequency (multi-decadal) fluctuations. The  
 610 black and red lines represent observations (CRU and GPCC, respectively), while the purple, green and orange  
 611 lines represent the ensemble means of ALL, fixEU, and their difference (EU). The grey shading represents the  
 612 standard deviation of the eight-member ALL ensemble around the mean. The 1901-1955 least-squares linear  
 613 trends of the simulated time series are shown as dashed lines in the corresponding colours.

614

615



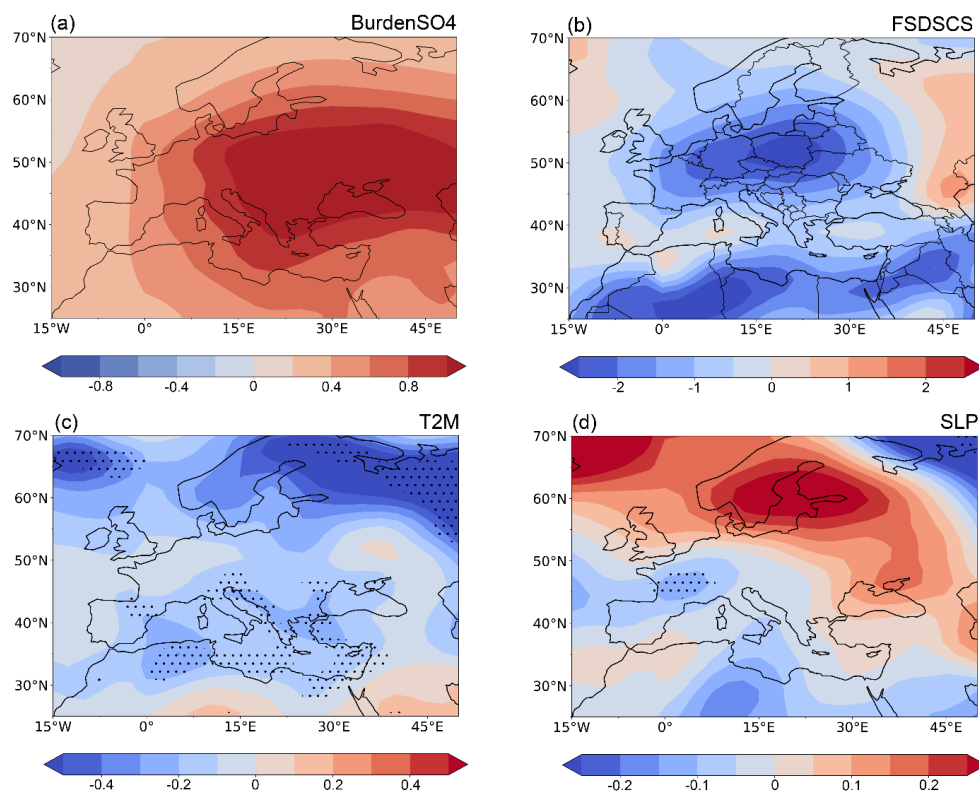
616  
 617

618 **Figure 2.** Spatial patterns of the 1901-1955 linear trends of the JJA average (a) 850-hPa winds ( $\text{m s}^{-1}$  (55 years)<sup>-1</sup>)  
 619 <sup>1</sup>) and 925-hPa streamfunction (colors,  $10^6 \text{ m}^2 \text{ s}^{-1}$  (55 years)<sup>-1</sup>), (b) 1000-300 hPa vertically integrated moisture  
 620 transport (vectors,  $\text{Kg m}^{-1} \text{ s}^{-1}$ ) and its divergence (shades,  $\text{mm d}^{-1}$  (55 years)<sup>-1</sup>), (c) 150-hPa divergent circulation  
 621 ( $\text{m s}^{-1}$  (55 years)<sup>-1</sup>) and its divergence (shades;  $10^{-6} \text{ s}^{-1}$  (55 years)<sup>-1</sup>) associated with increased European sulphate  
 622 aerosols (difference between the ALL and fixEU ensemble means). The black dots in (b) mark the grid points for  
 623 which the trend exceeds the 90% significance level according to the two-tailed Student's t-test.





624



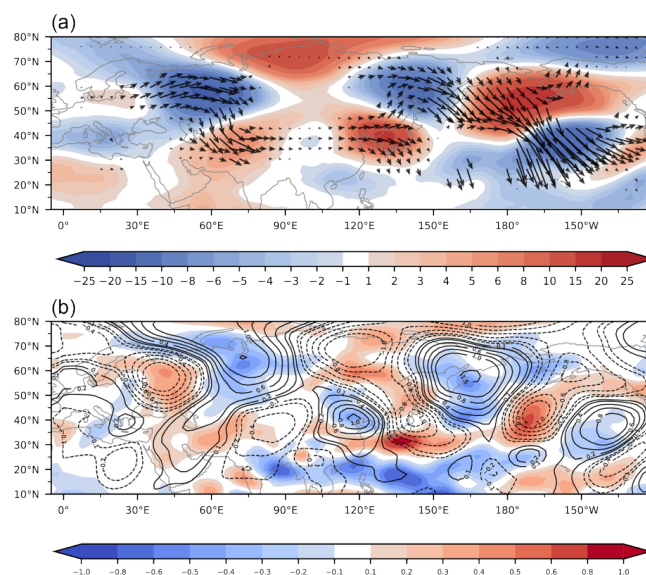
625

626

627 **Figure 3.** Spatial patterns of the 1901-1955 linear trends of the JJA average (a) column sulphate aerosol burden  
 628 ( $10^{-5} \text{ kg m}^{-2} (55 \text{ years})^{-1}$ ), (b) surface clear-sky downward shortwave radiation ( $\text{W m}^{-2} (55 \text{ years})^{-1}$ ), (c) 2-m air  
 629 temperature ( $\text{K} (55 \text{ years})^{-1}$ ), and (d) sea level pressure ( $\text{hPa} (55 \text{ years})^{-1}$ ) associated with increased European  
 630 sulphate aerosols (difference between the ALL and fixEU ensemble means). The black dots in (c) and (d) mark  
 631 the grid points for which the trend exceeds the 90% significance level according to the two-tailed Student's t-test.  
 632



633



634

635

636 **Figure 4.** Spatial patterns of the 1901-1955 linear trends of the JJA average (a) 300-hPa wave activity flux  
 637 (vectors;  $10^{-4} \text{ m}^2 \text{ s}^{-2} (55 \text{ years})^{-1}$ ) and streamfunction (shades;  $10^5 \text{ m}^2 \text{ s}^{-1} (55 \text{ years})^{-1}$ ), and (b) 300-hPa meridional  
 638 wind (contours;  $\text{m s}^{-1} (55 \text{ years})^{-1}$ ) and 500-hPa vertical velocity (shades;  $10^{-2} \text{ Pa s}^{-1} (55 \text{ years})^{-1}$ ) associated with  
 639 increased European sulphate aerosols (difference between the ALL and fixEU ensemble means).